Improved understanding of metal–graphene contacts

Improved understanding of metal–graphene contacts

F. Driussi[1*], S. Venica[1], A. Gahoi[2], A. Gambi[1], P. Giannozzi[1], S. Kataria[2], M.C. Lemme[2,3], P. Palestri[1], D. Esseni[1]

[1]*DPIA, Università degli Studi di Udine, via delle Scienze 206, Udine 33100, Italy;*
[2]*RWTH Aachen University, Aachen, Germany;*
[3]*AMO GmbH, Advanced Microelectronic Center, Aachen, Germany*

Abstract

Metal–graphene (M–G) contact resistance (R_C) is studied through extensive experimental characterization, Monte–Carlo transport simulations and Density Functional Theory (DFT) analysis. We show that the back–gate voltage dependence of R_C cannot be explained only in terms of the resistance of the junction at the edge between contact and channel region. Experiments and DFT calculations indicate a consistent picture where both Ni and Au contacts have a M–G distance larger than the minimum energy distance, and where the M–G distance is crucial in determining the R_C value.

Keywords: graphene, contacts, modeling, Monte-Carlo, DFT

1. Introduction

The excellent physical properties of graphene, such as high electron velocity and tunable optical absorption [1], make it suitable for many applications such as RF transistors [2], fast photodetectors [3], NEMS/MEMS and sensors [4], terahertz modulators [5], supercapacitors [6] and displays [7].

However, metal–graphene (M–G) contacts still exhibit large resistance (R_C), which is a major hindrance for graphene transistors as, for instance, it degrades severely the output conductance and the maximum oscillation frequency of graphene–FETs (GFETs) [2]. An improvement of R_C is thus mandatory to boost graphene technology [8].

The physical understanding is a prerequisite for the engineering of M–G contacts, but it is still partly lacking. Advanced modelling techniques [9] and first principle simulations [10], combined with a dependable experimental characterization [11] are the best options to understand and then improve the large R_C values of M–G contacts.

This work presents a comprehensive analysis of R_C for different M–G contacts that starts from experimental characterization based on the Transfer Length Method (TLM), and then leverages on Density Functional Theory (DFT) and semi–classical Monte–Carlo (MC) simulations. For the first time to our knowledge, a consistent picture is identified where the short (Ni contact) or long range nature (Au contact) of the M–G interaction and the actual M–G distance have a substantial influence on the R_C value.

2. Devices and experiments

Transfer Length Method structures (series of back–gated GFETs) with monolayer CVD graphene (G) and Ni, Cu and Au contacts were fabricated via photolithography. The complete fabrication description can be found in [12]. DC characterization was carried out at 300 K in ultra–high vacuum conditions (<10^{-6} mbar) to avoid air induced Dirac Point (DP) shifts and R_C extraction errors [13].

The total resistance R_T of GFETs was calculated from current (I_{DS}) versus back–gate voltage (V_{BG}) curves at fixed drain–source voltage (V_{DS}) as $R_T=V_{DS}/I_{DS}$. R_T consists of the channel sheet resistance (R_{SH}) and R_C:

$$R_T = R_{SH} L_{CH}/W + 2R_C$$

where W is the channel width and L_{CH} is the contact spacing. We extracted R_{SH} and R_C by linear fitting of R_T vs. L_{CH} experiments [11]. The average R_{SH} vs. V_{BG} curves (Fig. 1a) show that the graphene quality is similar and independent of the metal contacts. Data for the best device (lower R_{SH}, Au contact) are also reported. Instead, R_C depends on the metal (Fig. 1b), with larger values observed for Ni than for Au. Figure 1c shows that the G quality and R_C are correlated.

Typically, R_C consists of: a) the specific contact resistivity ρ_C, b) the R_{SK} of graphene underneath the contact, c) the R_{JUN} of the junction at the edge of the contact due to different G charge densities in the

* Corresponding author. *e.mail:* francesco.driussi@uniud.it

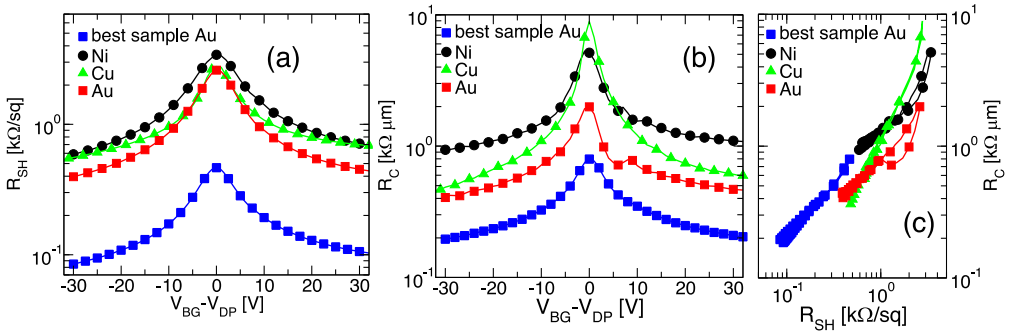

Fig.1. Extracted R_{SH} (a) and R_C (b) vs. V_{BG} for samples with Ni, Cu and Au contacts. Black/red/green symbols represent typical/average data; blue symbols are the best measured sample (Au contacts). (c) R_C versus R_{SH} correlation graph.

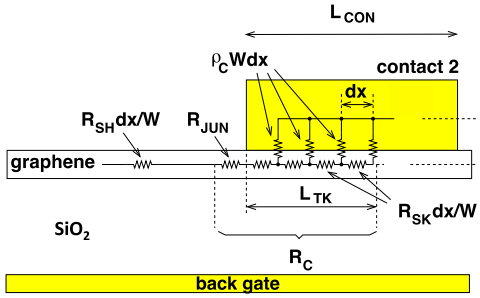

Fig.2. Contributions to the GFET resistance: in the channel (R_{SH}), at the contact edge (R_{JUN}) and below the contact (R_{SK}, ρ_C).

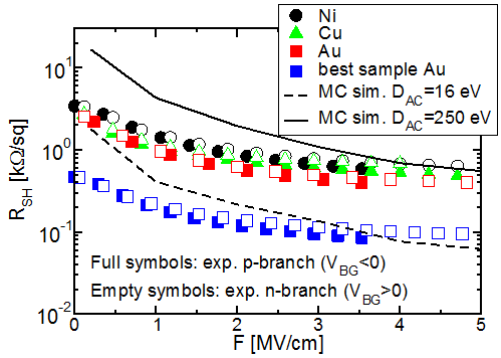

Fig.3. Experimental R_{SH} vs. back–oxide field (symbols) compared with MC simulations (lines) for two values of D_{AC}.

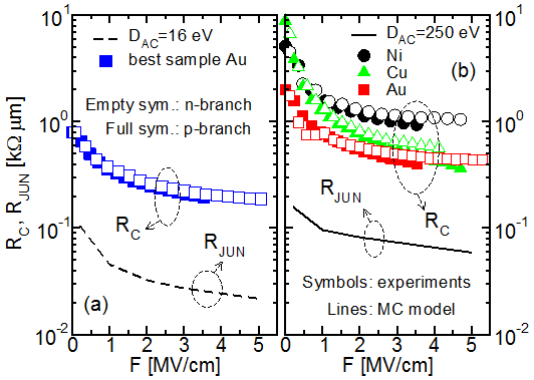

Fig.4. Experimental R_C (symbols) compared with R_{JUN} simulated with the MC model (lines) for two values of D_{AC}.

channel and contact region (Fig. 2). Metals are expected to electrostatically dope graphene [10], thus inducing fairly bias independent values of R_{SK} and ρ_C. Hence, the V_{BG} dependence of R_C has been mainly ascribed to the junction resistance R_{JUN}, because V_{BG} impacts the channel charge [11]. An alternative interpretation suggests the metal fails to dope graphene [14], thus V_{BG} affects R_{SK}, ρ_C and R_C itself. To discriminate between the two cases, we performed MC simulations of R_{JUN}.

3. Analysis of the R_C dependence on V_{BG}

We used a MC model that solves the Boltzmann transport equation for the 2D electron gas in graphene coupled to the Poisson equation. Scattering with acoustic and optical phonons in graphene and remote phonons in the back–oxide was considered [9].

To isolate the R_{JUN} contribution, the M–G stack enters the MC simulations only via the electrostatic potential: namely, the voltage drops across R_{SK} and ρ_C were neglected, so that

$$R_T = R_{SH} L_{CH}/W + 2R_C$$

and R_{SH} and R_{JUN} were extracted via linear fitting of the simulated R_T vs. L_{CH} curves. Figure 3 reports R_{SH} versus the back–oxide field F. The MC model reproduces the R_{SH} of the best device with standard G scattering parameters (dashed line) [15]. The larger measured average R_{SH} is presently unclear and, to the sole purpose of having the MC model reproducing the experiments, we empirically increased the deformation potential D_{AC} of acoustic phonons (solid line). Figure 4 compares the simulated R_{JUN} with measured R_C: R_{JUN} is only about one tenth of R_C. Hence R_{JUN} alone cannot explain the V_{BG} dependence of R_C, suggesting that also R_{SK} and ρ_C depend on V_{BG}. To verify the finding of the MS simulations, we applied the contact–end resistance method to the TLM samples [11]. The transmission line model links R_C to ρ_C, R_{SK} and the transfer length (L_{TK}, Fig. 2), so they can be obtained from the experiments (see Figs. 5 and 6).

The extracted R_{SK} has a marked V_{BG} dependence (Fig. 6, filled symbols). For Ni–G, R_{SK} is close to R_{SH} (Fig. 6a) and both agree with the simulation (line) of the G/oxide/back–gate stack in GFET channel [9]. This suggests Ni fails to dope graphene, which agrees with the very large ρ_C in Fig. 5b. Instead, Au does improve R_{SK} compared to R_{SH} (Fig. 6b) and also reduces ρ_C (Fig. 5b).

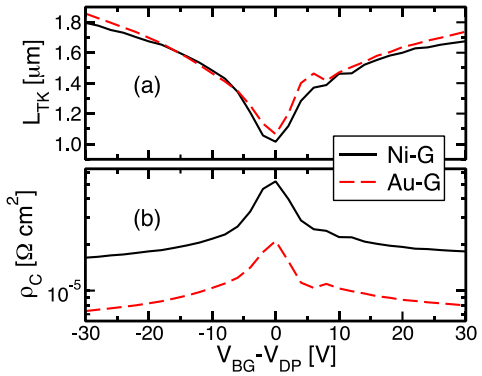

Fig.5. L_{TK} (a) and ρ_C (b) extracted from experiments for the Ni–G and Au–G contacts.

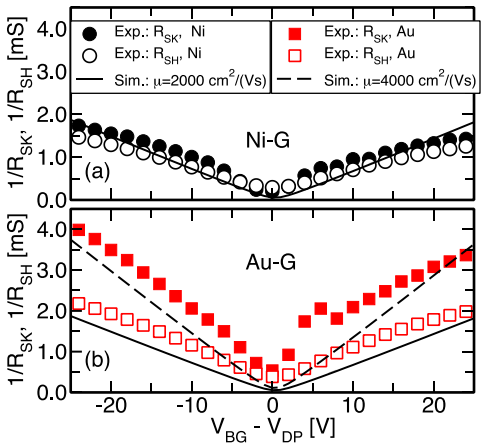

Fig.6. R_{SH} and R_{SK} (symbols) measured for Ni–G (a) and Au–G (b) and $R_{SH}=[\mu q(n+p)]^{-1}$ calculated for the G/oxide/back-gate system (lines). q is the elementary charge, n and p are electron and hole density, μ is the mobility.

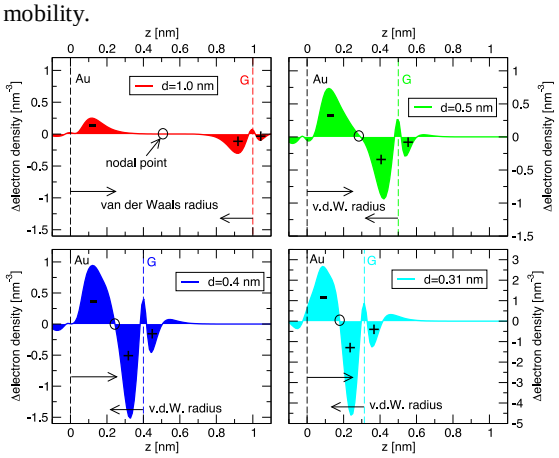

Fig.7. Induced net charge along z (perpendicular to graphene) for different Au–G distances. Dashed lines are the positions of atoms, while arrows are the van der Waals atomic radii.

3. DFT simulations of Au–G and Ni–G contacts

We performed DFT simulations of Ni–G and Au–G stacks by using Quantum ESPRESSO [16]. The 111 surface of Ni and Au crystals (3 layers) was matched to the G lattice [10]. For Ni–G, we considered a 1x1 graphene cell with a lattice constant of a=0.246 nm. For Au–G we matched the Au lattice with a 2x2 G

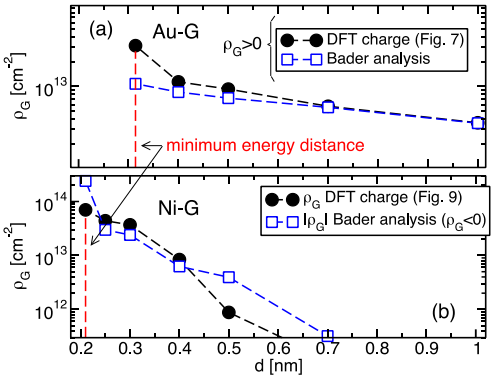

Fig.8. ρ_G vs. d in Au–G (a) and Ni–G (b), calculated by integrating the charges (circles) in Figs. 7 and 9 or via Bader analysis (squares). For Au–G the ρ_G extraction techniques agree. ρ_G extraction is more complex in Ni–G, showing also a shorter–range interaction than Au–G.

supercell [10]. Local–spin density approximation, plane–wave basis sets and gradient–corrected exchange–correlation functional (PBE) were used for Ni, Au and C atoms. Van der Waals interactions and dipole correction were considered [16]. In the simulations, we varied the M–G distance d and the minimum energy distance for Au–G (d=0.31 nm) and Ni–G (d=0.21 nm) are obtained by force minimization.

3.1. The Au–G contact

To analyze the graphene doping due to the Au contact, we calculated the difference between the valence electron density of the Au–G stack and the isolated Au and G layers [17]. Figure 7 shows the results averaged over the graphene plane: by lowering d, positive charge accumulates near the graphene, while negative charge builds up near Au. To evaluate the graphene doping (ρ_G), we integrated these dipoles along z (perpendicular to graphene) up to the nodal points (circles, Fig. 7).

To exclude possible contributions by the charge redistribution due to Pauli repulsion [17], we also calculated the charge variation of each C atom induced by the Au proximity via Bader analysis [18]. Bader charges (Fig. 8a, squares) agree well with the dipole integration (circles), except at d=0.31 nm; in this case d is shorter than the sum of the Au and C atomic radii (Fig. 7), so Au and C charges are largely overlapping at a given z, precluding a meaningful determination of ρ_G via dipole integration. Fig. 8a shows that graphene is p–doped by Au for distances up to 1 nm, revealing a long–range interaction.

3.2. The Ni–G contact

We repeated the analysis also for the Ni–G stack. Figure 9 shows a more complex Ni–G interaction (several dipoles along z); thus, it is difficult to discriminate between Ni and G charges. The integration of the charge up to the nodal point closest to graphene (circles, Fig. 9) leads to a p–doping of

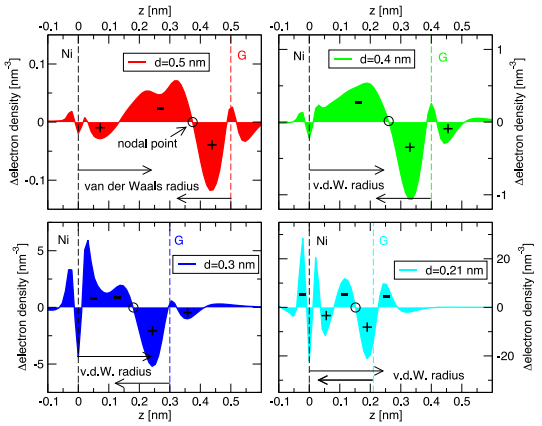

Fig.9. Induced net charge along *z* (perpendicular to graphene) for different Au–G distances. Dashed lines are the positions of atoms, while arrows are the van der Waals atomic radii.

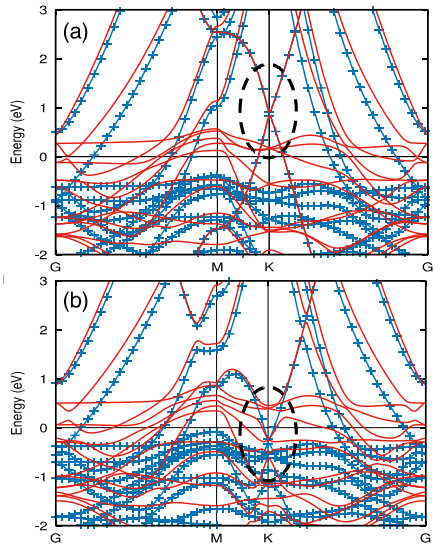

Fig.10. (a) *d*=0.5 nm: energy bands of Ni-G stack are the superimposition of Ni and G bands: Dirac cone is visible at the *K* point. (b) *d*=0.3 nm: Ni induces gaps in graphene and Dirac cone vanishes. Blue lines are for spin up, red lines are for spin down.

graphene (ρ_G>0, Fig. 8b, circles). Bader charges reveal, instead, a *n*–doping (ρ_G<0, squares).

Concerning this discrepancy, in Fig. 9, van der Waals radii of Ni and C largely overlap for *d*<0.4 nm, which makes the dipole analysis inadequate to determine ρ_G for the Ni–G stack. In this respect, the energy band diagrams of Ni–G in Fig. 10 support this picture. For *d*=0.5 nm, the bands of the Ni–G system still resemble the bands of Ni and graphene alone (Fig. 10a) and, in particular, the Dirac cone of graphene can be recognized at the *K* point. Instead, when *d* is reduced to 0.3 nm (b), the Dirac cone disappears, opening of an energy gap [10], so it is difficult to interpret the Ni–G stack in terms of a Ni and a G sub–systems.

However, the Ni–G interaction vanishes for *d*>0.5 nm (Fig. 8b), leading to $|\rho_G|<10^{12}\text{cm}^{-2}$ and suggesting a shorter–range interaction compared to Au–G. This explains the experiments in Fig. 6: Ni fails to dope graphene ($R_{SK} \simeq R_{SH}$), probably because of an ineffective Ni–G distance (e.g. *d*>0.5 nm), whereas Au does improves R_{SK} compared to R_{SH} (Fig. 6b), most likely because the longer–range interactions enable a G doping despite a possible not optimal Au–G distance.

4. Conclusions

Ni has a strong chemical interaction with graphene at the minimum energy distance, which however vanishes for Ni–G distances larger than 0.5 nm. Experiments show a large and strongly V_{BG} dependent R_C, suggesting that Ni fails to effectively dope graphene and a Ni–G distance larger than 0.5 nm.

For Au–G contacts, a longer–range interaction and significant G doping are predicted for distances up to 1 nm, which explains the lower experimental R_C compared to the Ni–G contact.

Acknowledgements

Work was funded by the EU through the FP7 STREP Project "GRADE" (317839) and an ERC grant (InteGraDe, 307311). German Research Foundation is acknowledged.

References

[1] A. K. Geim, Science. 324 (2009) 1530-1534, https://doi.org/10.1126/science.1158877.

[2] Y. Wu, et al., ACS Appl. Mat. & Interfaces. 8 (2016) 25645-25649, https://doi.org/10.1021/acsami.6b0579.

[3] S. Riazimehr et al., Solid-State Electronics. 115 (2016) 207-212, https://doi.org/10.1016/j.sse.2015.08.023.

[4] A. D. Smith, et al., Nano Letters. 13 (2013) 3237-3242, https://doi.org/10.1021/nl401352k.

[5] B. Sensale-Rodriguez et al., Nature Communications. 3 (2012) 780, https://doi.org/10.1038/ncomms1787.

[6] C. Liu, et al., Nano Letters. 10 (2010) 4863-4868, https://doi.org/10.1021/nl102661q.

[7] J. K. Wassei and R. B. Kaner, Materials Today. 13 (2010) 52-59, https://doi.org/10.1016/S1369-7021(10)70034-1.

[8] A. Meersha, et al., IEDM Tech. Digest. (2016) 5.3.1-5.3.4, https://doi.org/10.1109/IEDM.2016.7838352.

[9] S. Venica, et al., Proceedings of SISPAD. (2016) 357-360, https://doi.org/10.1109/SISPAD.2016.7605220.

[10] P. A. Khomyakov, et al., Phys. Rev. B. 79 (2009) 195425, https://doi.org/10.1103/PhysRevB.79.195425.

[11] S. Venica, et al., IEEE Transaction on Electron Devices. 65 (2018) 1589-1596, https://doi.org/10.1109/TED.2018.2802946.

[12] A. Gahoi, et al., Solid–State Electronics. 125 (2016) 234-239, https://doi.org/10.1016/j.sse.2016.07.008.

[13] S. Venica, et al., Proceedings of ICMTS. (2018) 57-62, https://doi.org/10.1109/ICMTS.2018.8383765.

[14] Z. Chen, et al., Proc. of Symposium on VLSI Technology. (2009) 128-129.

[15] M. Bresciani, et al., Solid State Electronics. 54 (2010) 1015-1021, https://doi.org/10.1016/j.sse.2010.04.038.

[16] P. Giannozzi et al., J. Phys. Condens. Matter. 29 (2017) 465901, https://doi.org/10.1088/1361-648X/aa8f79.

[17] C. Gong, et al., Journal of Applied Physics. 108 (2010) 123711, https://doi.org/10.1063/1.3524232.

[18] G. Henkelman, et al., Comp. Material Science. 36 (2006) 354-360, https://doi.org/10.1016/j.commatsci.2005.04.010.